



Title	Origin of the intense positive and moderate negative atmospheric electric field variations measured during and after Antarctic blizzards
Author(s)	Minamoto, Yasuhiro; Kamogawa, Masashi; Kadokura, Akira; Omiya, Satoshi; Hirasawa, Naohiko; Sato, Mitsuteru
Citation	Atmospheric research, 263, 105812 https://doi.org/10.1016/j.atmosres.2021.105812
Issue Date	2021-12-01
Doc URL	http://hdl.handle.net/2115/90848
Rights	©2021. This manuscript version is made available under the CC-BY-NC-ND 4.0 license http://creativecommons.org/licenses/by-nc-nd/4.0/
Rights(URL)	http://creativecommons.org/licenses/by-nc-nd/4.0/
Type	article (author version)
File Information	Atmos. Res. 263_105812.pdf



[Instructions for use](#)

1 Origin of the intense positive and moderate negative atmospheric electric
2 field variations measured during and after Antarctic blizzards

3
4 Yasuhiro Minamoto, Masashi Kamogawa, Akira Kadokura, Satoshi Omiya,
5 Naohiko Hirasawa, Mitsuteru Sato
6

7 **Corresponding author**

8 Masashi Kamogawa

9 kamogawa@u-shizuoka-ken.ac.jp

10 Global Center for Asian and Regional Research, University of Shizuoka

11 3-6-1, Takajo, Aoi-Ku, Shizuoka-City, Shizuoka Prefecture, 420-0839, Japan
12

13 **Abstract**

14 There is an atmospheric electric field (AEF) or an electric potential gradient (PG) in fair weather
15 between the Earth's surface and the mesosphere/ionosphere, which is positive. During
16 blizzards/snowstorms in the polar regions, an intense positive AEF/PG in the order of 10^3 V/m of
17 the same polarity in fair weather was observed using an electric field mill at 1.4 m in height. In
18 contrast, a moderately negative AEF/PG variation after a blizzard was observed in 2015 at Syowa
19 Station, Antarctica. The negative variation, where the magnitude ranged from tens to hundreds of
20 V/m, gradually recovered into the positive AEF/PG for more than 40 minutes. According to various
21 studies on blowing/drifting snow dynamics and electricity in laboratory experiments and field
22 observations, snow particles colliding with the snow surface are charged, and the charge of saltating
23 and suspended particles during the snowstorm is negative on average. To verify the AEF/PG
24 observed during and after the blizzards, we numerically estimated the electric field surrounding the
25 conductive sensor unit of the electric field mill using a three-dimensional Poisson equation. Under
26 blizzard conditions, the polarity of the estimated AEF/PG was the opposite of that of the observed
27 AEF/PG. From the noise study of the field mill, we deduced that the positive AEF/PG variations
28 were caused by the collision of negatively charged snow particles with the electric probe on the
29 sensor unit. Just after the blizzard, the number of snow particles measured at 4.4 m in height clearly
30 decreased, and the camera image showed clear visibility. From this evidence, we modeled the
31 suspended and saltating negatively charged snow particles that had fallen onto the ground surface
32 and then constructed a charge layer of the snow particles softly attaching to the ground, which
33 slowly discharged following the study on the electrical resistance of the powders. The three-
34 dimensional Poisson calculation based on the model reproduced a moderately negative AEF/PG.
35 Thus, we elucidated that the origins of the intense positive and moderate negative electric fields
36 during and after blizzards are the charged snow particles colliding with the electric probe on the
37 sensor unit and the negative snow layers softly attached to the ground, respectively. These results

38 are applicable to studies on dust storm electrification on Mars' and Earth's deserts, snowstorm
39 electrification in the polar regions, and high mountains, such as Mt. Fuji in Japan, and turbulent
40 electrification for industrial dust, which provides the identification of intense electrification and
41 storms.

42

43 **Keywords**

44 Atmospheric electric field; Potential gradient; Electric field mill; Blizzard; Antarctica; Charged
45 snow particles.

46

47 **1. Introduction**

48 There is an atmospheric electric field (AEF) in fair weather between the Earth's surface
49 and the mesosphere/ionosphere. The magnitude of the AEF at the ground surface is around 100
50 V/m in fair weather at sea level (MacGorman and Rust, 1998; Harrison, 2013; Williams and
51 Mareev, 2014). The AEF transports atmospheric ions originating from atmospheric molecules
52 ionized by cosmic rays and natural radionuclides as air-earth currents (i.e., a weak electric current
53 flow from the mesosphere/ionosphere to the ground surface). Negative charges are transported
54 from the negatively polarized bottom of clouds to Earth's surface via negative ground-to-ground
55 lightning, which occurs constantly all over Earth. The positive charges in thunderclouds are
56 transported into the mesosphere/ionosphere, generating an electric potential difference in relation
57 to Earth. The negatively charged precipitation also transports negative charges to Earth's surface
58 (Liu et al., 2010). This electrical circuit on Earth is called the global electrical circuit
59 (MacGorman and Rust, 1998; Harrison, 2004; Williams and Mareev, 2014). The electric potential
60 difference between Earth's surface and the mesosphere/ionosphere, which forms a massive
61 global-scale spherical capacitor, is around 250 kV (Markson, 2007). The downward (geocentric
62 direction) of the vertical AEF is conventionally defined as positive. In other words, it is a positive
63 AEF under fair-weather conditions. This definition is adopted in many studies of atmospheric
64 electricity and many papers.

65 With the electric field vector and the electric potential expressed as E and V , respectively,
66 E is given as follows:

$$67 \quad \mathbf{E} = -\nabla V. \quad (1)$$

68 When only the vertical z -axis is discussed, as in the case of the AEF in fair weather, equation (1)
69 is expressed as follows:

$$70 \quad E_z = -\frac{dV}{dz}. \quad (2)$$

71 Here, we introduce the electric potential gradient (PG), which is a scalar quantity:

$$72 \quad \text{PG} = E_z. \quad (3)$$

73 In this case, PG and E_z have the same magnitude. Therefore, PG has also been used in some papers

74 as a general expression because it is positive, like the AEF in fair weather (e.g., Harisson, 2013;
75 Aplin, 2018; Nicoll et al., 2019). The present paper follows this definition for AEF/PG unless
76 otherwise noted.

77 According to the World Meteorological Organization (1966), blowing snow was defined
78 as snow raised by the wind to moderate heights above the ground, reducing horizontal visibility at
79 eye level. The same source defined a snowstorm as a meteorological disturbance giving rise to a
80 heavy fall of snow, often accompanied by strong winds, and a blizzard as a violent winter storm
81 lasting at least 3 hours. It is combined with below-freezing temperatures and extremely strong wind
82 laden with blowing snow, which reduces visibility to less than 1 km. Blizzards at Syowa Station,
83 Antarctica (69°00'S, 39°35'E) have been identified by the criteria described in Sato and Hirasawa
84 (2007), including visibility of less than 1 km and wind velocity of more than 10 m/s continuing for
85 more than 6 hours. The blizzard at Syowa Station is regarded as a weather event as defined by these
86 criteria.

87 In blowing snow conditions, including snowstorms and blizzards, an intense positive
88 AEF/PG accompanied by high-frequency fluctuations was observed using an electric field mill.
89 Gordon and Tylor (2009) measured the AEF/PG for 80 days in Amundsen Bay, Canada (70°03'N,
90 126°18'W) and observed intense positive variations of the AEF/PG during blowing snow events.
91 In a polar observation, Kikuchi (1970) reported an intense positive AEF/PG observed during a
92 blizzard at Syowa Station. Although the wind velocity and magnitude of the AEF/PG were
93 correlated in previous studies (e.g., Kikuchi, 1970; Gordon and Tylor, 2009), the origin of the
94 positive AEF/PG was unclear.

95 The dynamics of blowing snow involve the dynamics of snow drifting near the snow
96 surface. During snow drifting, the dynamics of snow particles produces an electrical charge,
97 categorized into the following three modes: saltation, suspension, and surface creep (Nemoto and
98 Nishimura, 2004). Saltation refers to snow bouncing at the snow surface and/or pushing one
99 particle out of another; suspension refers to snow migrating without touching the ground surface;
100 and creeping refers to snow migrating, frequently in contact with the snow surface. When a
101 snowstorm begins, the snow particles on the snow surface migrate as the wind speed increases,
102 causing creep. The creep of the particles develops into saltation, which generates suspension
103 (Anderson, 1987; Nemoto and Nishimura, 2004). When the snowstorm terminates, the suspended
104 and saltating particles diminish.

105 Snow particles that collide with the snow surface are charged. Maeno et al. (1985)
106 executed a laboratory experiment to collide positively and negatively charged snow seeds with
107 snow surfaces under horizontal wind blowing inside a horizontal wind tunnel. The blowing snow
108 particles were negatively charged, regardless of the initial seed polarity. The charge-to-mass ratio
109 of the snow particles after the collision was -0.1 to -0.3 $\mu\text{C}/\text{kg}$. As described below, the amount
110 of negative charge measured in the laboratory experiment was two orders of magnitude smaller

111 than that observed in the field. Omiya and Sato (2011) examined the correlation between the
112 electric charge of snow particles and their saltation in the same type of laboratory experiment as
113 Maeno et al. (1985). They showed that the negative charge of snow particles accumulated with an
114 increase in saltation occurrences. This means that the saltation in the laboratory experiments was
115 smaller than that in the field because of the limited length of the wind tunnel.

116 In 1967 and 1968, Wishart (1968) measured the amount of charge on snow particles
117 during the snowstorms at Byrd Station, Antarctica (80°00'S, 119°30'W), using a Faraday cage and
118 a charge electrometer. He conducted two observation campaigns for different height measurements.
119 The first observation showed that the charge-to-mass ratio of snow particles ranged from -1.4 to
120 -7.7 $\mu\text{C}/\text{kg}$ at a wind velocity of 4.5 to 6.5 m/s in an air temperature of -5 to -6°C and a height of
121 50 cm; this corresponded to a wind velocity of 6.5 to 9 m/s at a height of 10 m. The second
122 observation showed that the charge-to-mass ratio comprised roughly negative constant
123 values, -0.05 $\mu\text{C}/\text{kg}$ at a wind velocity of 4.5–6.5 m/s, air temperature of -9 to -12°C (snow
124 temperature of -10 to -13 C), and height of 15 cm, corresponding to a wind velocity of 7.5–9 m/s
125 and a height of 10 m. Schmidt et al. (1999) measured the charge amount of 11 individual drifting
126 snow particles at Chimney Park, Wyoming, USA, and measured both positive and negative charges.
127 The charge-to-mass ratios of six negatively charged snow particles and five positively charged
128 snow particles ranged from -12 to -208 $\mu\text{C}/\text{kg}$ and 1 to 72 $\mu\text{C}/\text{kg}$, respectively. Burrows and Hobbs
129 (1970) measured the charge of 3,654 snow particles passing through an induction coil during a
130 light snowfall at an altitude of 2,025 m on Mt. Olympic, Washington, USA, and showed that the
131 proportions of positively and negatively charged snow particles were 52% and 48%, respectively.
132 The charge amounts per snow particle were on the order of 10^{-14} to 10^{-12} C. In Sapporo, Japan,
133 Asuma et al. (1988) measured the electric charge of individual precipitation particles on the ground
134 and at altitudes of 100 m and 200 m using a moored balloon at a wind speed of less than 6 m/s.
135 They showed that positively and negatively charged precipitation particles were dominantly found
136 in the sky and near the ground surface, respectively. The charge amounts per snow particle were in
137 the order of 10^{-13} to 10^{-12} C. Therefore, both the positively and negatively charged snow particles
138 were measured for suspended snow particles in the field observations. However, the dominant
139 charge was statistically negative for the particles that were saltating and suspended during
140 snowstorms in field observations (Wishart, 1968; Latham and Montagne, 1970; Schmidt et al.,
141 1999).

142 The studies described above have shown that although snow particles in wind tunnel
143 experiments controlled for saltation were negatively charged, both positively and negatively
144 charged particles were observed in the snow particles where saltation could not be confirmed in
145 the field. The charge-to-mass ratios of the particles observed in the field observations were two
146 orders of magnitude larger than those measured in the laboratory experiments. These results
147 suggest that collisions between the snow particles and the snow surface should generate a larger

148 negative charge accumulation on the particles; they imply that the difference in charge-to-mass
149 ratios between field and laboratory experiments was caused by the difference in the number of
150 collisions owing to the different lengths of saltation.

151 Negative (upward) AEF/PG has been observed on the ground when the polarity of the
152 dominant charge above the field mill is negative, such as in thunderstorm events (e.g., Suzuki et
153 al., 2011). Similarly, multiple negatively charged snow particles during the snowstorm were
154 suspended around the sensor unit of the electric field mill that measured AEF/PG. Therefore, one
155 may surmise that the electric field direction was from the electrical probe of the sensor unit to the
156 negatively charged snow particles. In this case, the measured value was negative, as was the case
157 just below the thundercloud. It is not clearly understood why positive AEF/PGs were measured
158 during the blizzard/snowstorm.

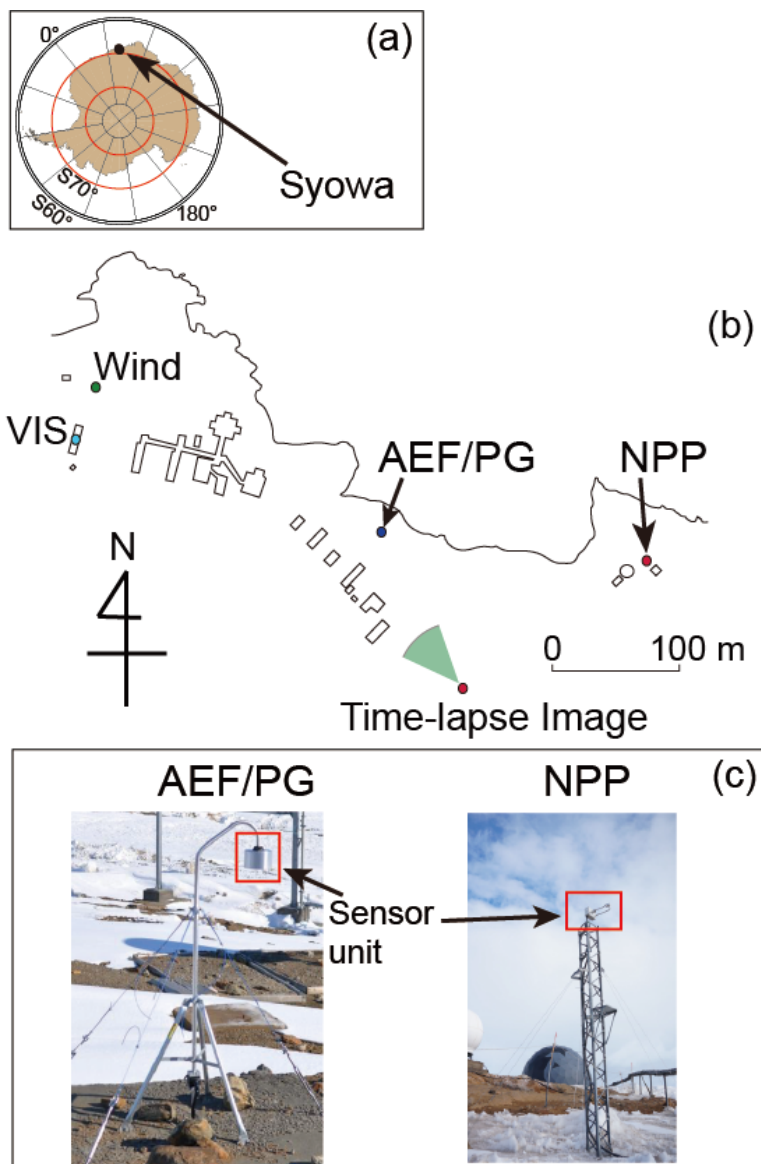
159 An intense positive AEF/PG exceeding 10 kV/m was reported at Syowa Station during
160 blizzards (Kikuchi, 1970). In addition, as described below, a moderate negative AEF/PG of -30
161 to -110 V/m was observed with a duration of 50 to 100 minutes, just after the blizzard on several
162 occasions. In this study, we show the time series of the AEF/PG, the wind velocity, and the number
163 of snow particles during the intense positive AEF/PG in the blizzard, as well as the moderate
164 negative AEF/PG just after the blizzard. Furthermore, we demonstrated the numerical calculation
165 of the AEF/PG formed by the distribution of the negatively charged snow particles to investigate
166 the origin of the positive and negative AEF/PG variations during and after the blizzard, respectively.
167 We discuss how to construct the intense positive AEF/PG during the blizzard and the moderate
168 negative AEF/PG just after the blizzard.

169

170 **2. Observation**

171 In this study, we used the data of the AEF/PG, the wind velocity, the number of
172 precipitation particles (NPP), and still images recorded by a live camera at Syowa Station in 2015.
173 Syowa Station is located on East Ongul Island, about 4 km east of Antarctica. Fig. 1 shows the
174 location of Syowa Station and the observation points in the station. The electric field mill measures
175 the magnitude and polarity of the AEF/PG estimated from the amount of electric charge on the
176 electrical probes (stators), which are alternately shielded and exposed by a grounded rotor
177 (MacGorman and Rust, 1998). We used a Boltek EFM-100 electric field mill to observe the
178 AEF/PG. The time resolution of the measurement was 2 Hz; the median value of 120 measured
179 values was taken as 1-minute representative values for the analysis. The sensor unit was installed
180 at a height of 1.4 m, and the electric probe of the sensor unit faced not the zenith but the ground
181 (an inverted sensor) to avoid noise originating from snow precipitation and rainfall.

182



183

184 Fig. 1. (a) Location of Syowa Station, Antarctica, (b) observation points in the station, and (c)
 185 sensor photos of the atmospheric electric field (AEF)/potential gradient (PG) and the number of
 186 precipitation particles (NPP). The AEF/PG and NPP in (b) denote the location of the electric field
 187 mill to observe the AEF/PG and the laser precipitation monitor (LPM) sensor to observe the
 188 number and size of precipitation particles, respectively. The time-lapse image and the wind indicate
 189 the live camera and the location of the wind velocity sensor, respectively. Visibility (VIS) denotes
 190 the observation point for visibility.

191

192 The AEF/PG measured by an electric field mill does not correspond to the ambient
 193 AEF/PG in fair weather because the electric lines of force are concentrated around the conductive
 194 field-mill sensor, causing the intense AEF/PG. In addition, the electric conductive environment
 195 around the sensor also modulates the AEF/PG around the sensor. Hence, in general, the calibration

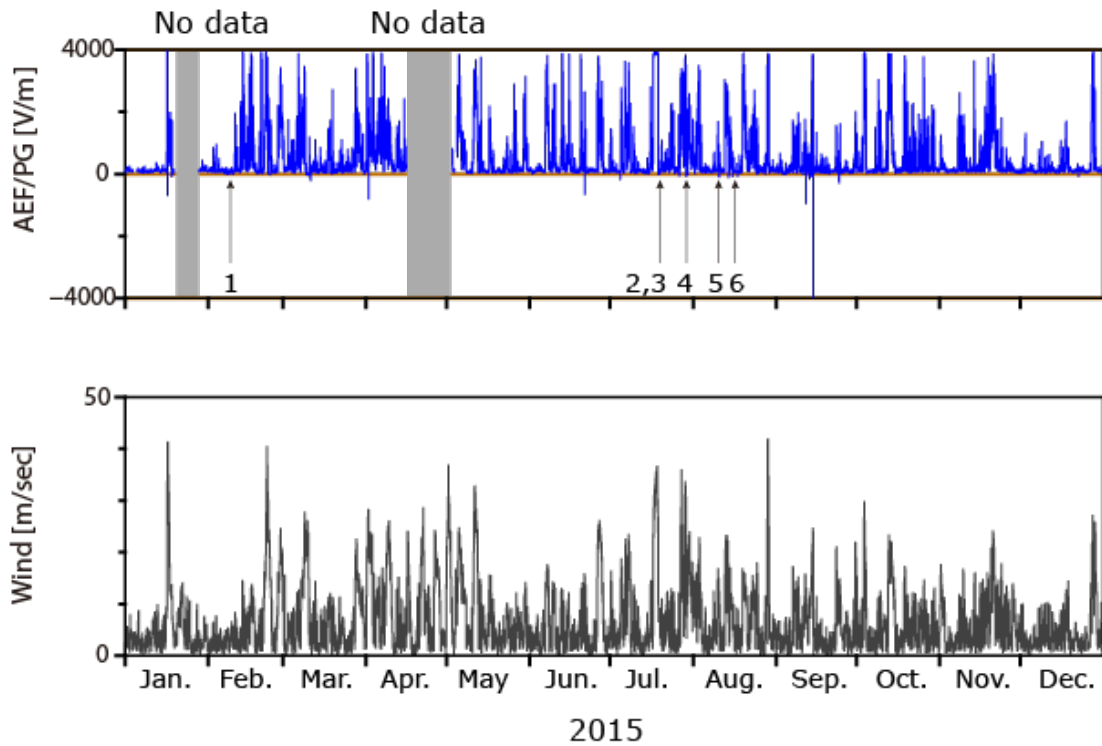
196 is conducted, comparing the field mill for the observation and the field mill embedded in the ground
197 (See Tsurudome et. al, 2013). Note that this calibration is effective for fair-weather observation and
198 thunderstorms with a high cloud bottom. The calibration factor of the field mill for the present
199 study (0.20) was obtained by the comparative observations described in MacGorman and Rust
200 (1998). The measurement range of the present field mill was ± 20 kV/m. Therefore, the observed
201 range of AEF/PG was $\pm 4,000$ V/m, which is ± 20 kV/m multiplied by the calibration factor.

202 The wind velocity data were 1-minute data provided by the Japan Meteorological Agency.
203 The NPP, by size, was measured using a laser precipitation monitor (LPM). The sensor was
204 installed at a height of 4.4 m. When the particles fell through the laser sheet between the laser
205 emission part and the intensity detector, the size of the laser shadow behind the particles one by
206 one was measured (Hirasawa et al., 2018). In this study, we used the 1-minute data of the number
207 of particles and assessed the number of particles in the different classes measured as a distribution
208 of snow particles before, during, and after the blizzard. The diameter of the precipitation particles
209 was recorded as 22 diameter classes (i.e., 22 bins) by the LPM. However, we recategorized the
210 particle diameter into the following four classes, because the major diameter of the precipitation
211 particles was less than 0.500 mm: 0.125 mm or less, 0.250 mm or less, 0.375 mm or less, and more
212 than 0.375 mm.

213 Regular observations of visibility were carried out eight times a day (i.e., every 3 hours).
214 When there was an abrupt change in the weather, such as before and after the blizzard, a temporary
215 observation was also conducted. To confirm the blizzard, we used time-lapse images provided by
216 the live camera recording every 5 minutes (Figs. 5 and 7), which was installed 140 m away from
217 the AEF/PG observation point (Fig. 1). The visibility to identify the blizzard was ocularly observed
218 500 m away from the live camera. In addition, visibility was not measured in a specified direction
219 but in the direction with the most visibility. Therefore, the view direction of the live camera did not
220 always coincide with that of the visibility observation. This may have caused differences in the
221 timing of the start/end of the blizzard between the ocularly assessed visibility and the still images
222 recorded by the live camera.

223 Fig. 2 shows the time series of the AEF/PG variations observed at Syowa Station from
224 January to December 2015. Positive AEF/PGs were frequently observed, whereas negative electric
225 fields were only occasionally seen. A positive AEF value exceeding 1 kV/m often lasted for several
226 hours, whereas a negative value rarely lasted for more than 1 hour. Fig. 3 shows the relationship
227 between the wind velocity and the AEF/PG from January to December 2015. As the wind velocity
228 increased, the AEF/PG value and its variability increased. Indeed, below a wind velocity of 6 m/s,
229 the AEF/PG value and its variability were smaller than those of the large wind velocity. Minamoto
230 and Kadokura (2011) employed a threshold of 6 m/s for the criteria to identify fair-weather
231 conditions. We note that when the wind velocity exceeded 26 m/s, the values of the 75th and 90th
232 percentiles of the observed values were almost equivalent because of the saturation of the

233 measurement.



234

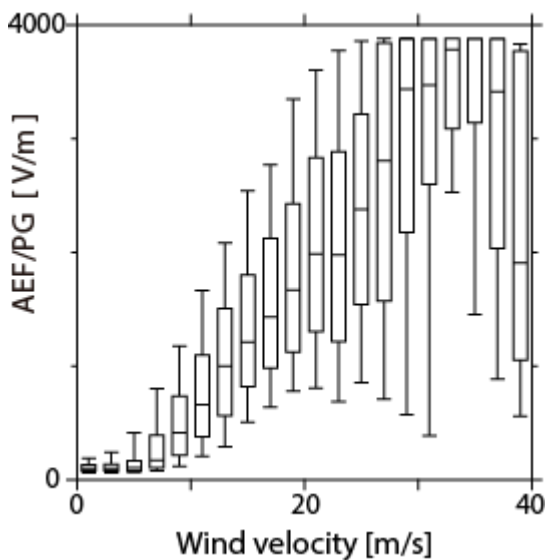
235 Fig. 2. Time series of 1-minute data of the AEF/PG and wind velocity in 2015 at Syowa Station.

236 There are two data gaps, which are in January and from the middle of April to the beginning of

237 May. The numbers below the AEF/PG panel correspond to the events of negative AEF/PG

238 variations after the blizzard, as listed in Table 1.

239



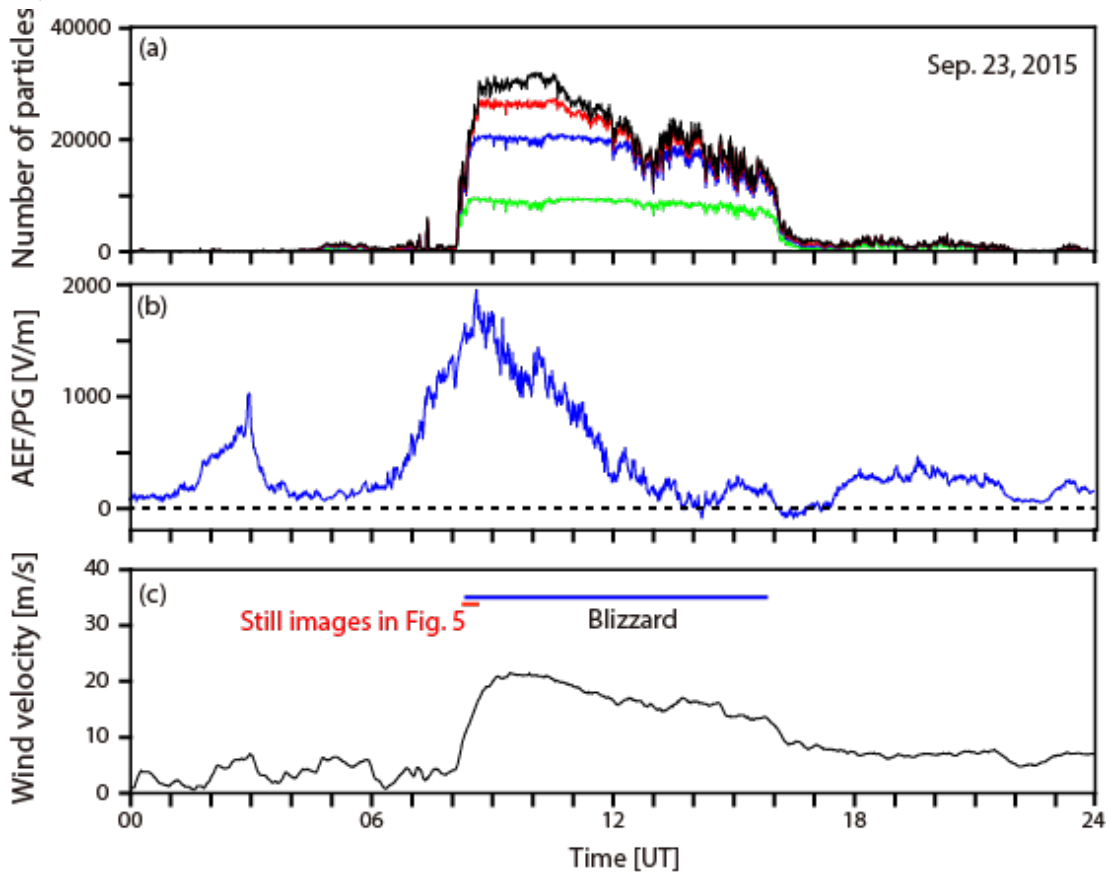
240

241 Fig. 3. Box-and-whisker plot for the relationship between wind velocity and the AEF/PG from

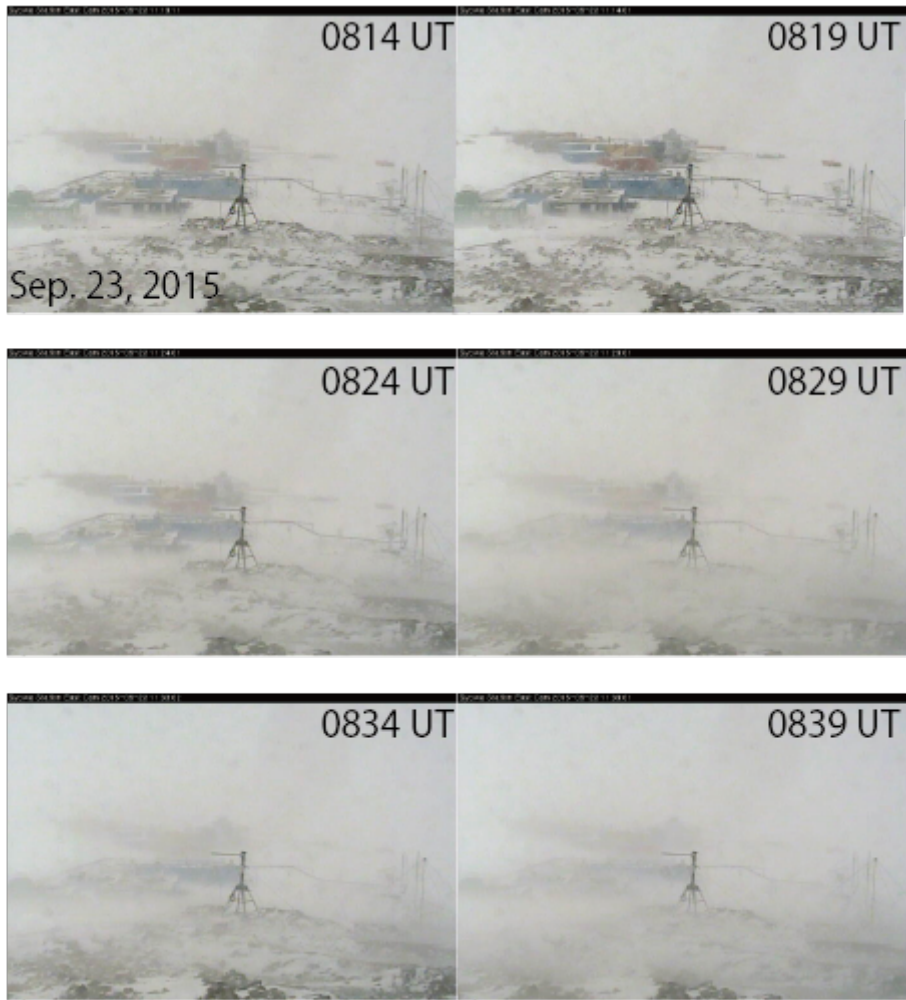
242 January to December 2015. The whiskers and downside/middle/upside of the box indicate 10th,

243 25th, 50th, 75th, and 90th percentile values from the bottom. The class width of the wind velocity

244 was 2 m/s. The upper limit corresponding to a saturated value of the AEF/PG measurement was
245 +4,000 V/m.



246
247 Fig. 4. Number of particles, AEF/PG, and wind velocity of 0 UT to 24 UT on September 23, 2015.
248 (a) Number of particles in different particle size classes. The green, blue, red, and black lines
249 indicate the number of particles with a diameter of 0.125 mm or less, 0.25 mm or less, and 0.375
250 mm or less, as well as the total number of particles. (b) AEF/PG. (c) Wind velocity. The blue and
251 red bars denote the period of the blizzard and still images shown in Fig. 5, respectively.



252
 253 Fig. 5. Still images recorded every 5 minutes by the live camera from 0814 UT to 0839 UT on
 254 September 23, 2015.

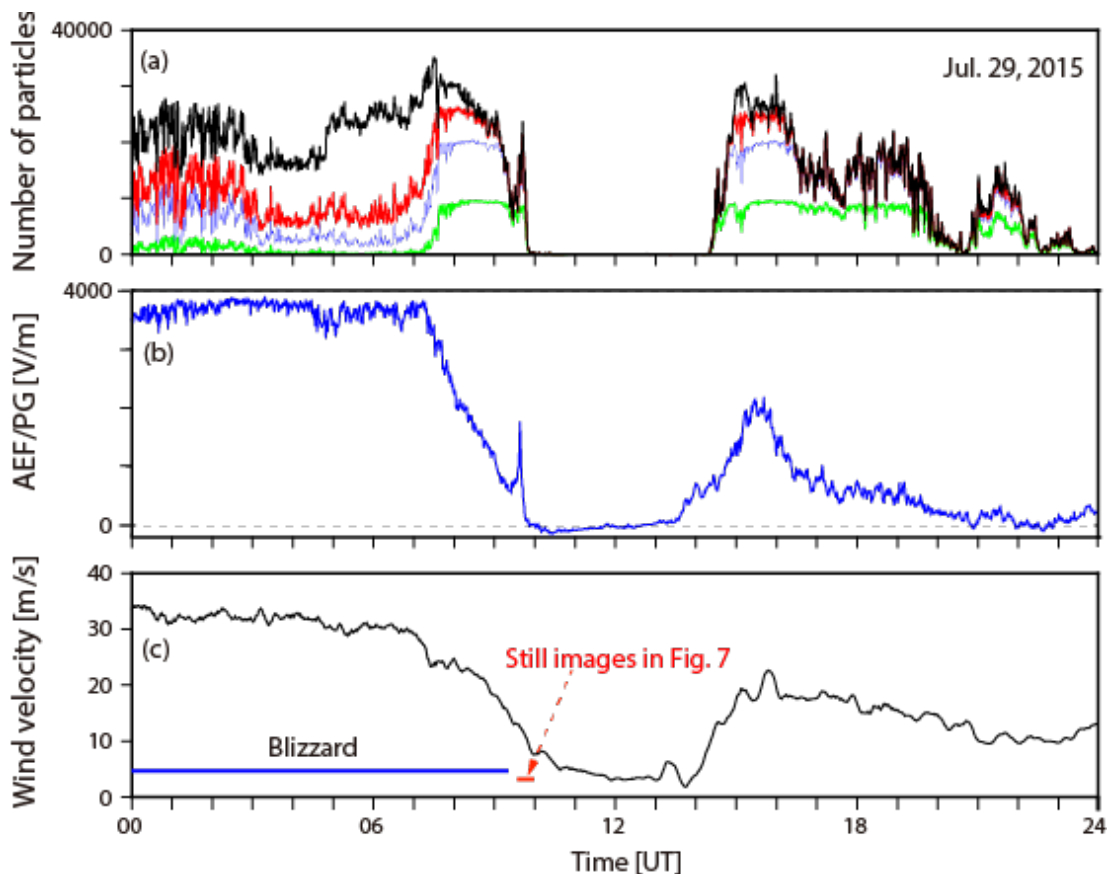
255
 256 Fig. 4 shows the time series of the number and size of snow particles, AEF/PG, and wind velocity
 257 on September 23, 2015, as an example of a blizzard period. The start and end of the blizzard were
 258 recorded at 0818 UT and 1550 UT, respectively (Oshiki, 2016). The wind velocity exceeded 6 m/s
 259 at 0810 UT and reached 20 m/s at 0900 UT. The AEF/PG and the number of particles increased
 260 rapidly around 0630 UT and 0700 UT, respectively. Note that we did not describe the origin of the
 261 enhancement of AEF/PG around 0300 UT not related to the increase in the number of snow
 262 particles and the wind. The origin was unknown, and similar variations were barely observed. Fig.
 263 5 shows the still image of the live camera recording every 5 minutes from 0814 UT to 0839 UT on
 264 September 23, 2015. The visibility dropped between 0819 UT and 0824 UT. When the blizzard
 265 started at 0818 UT, the wind velocity was 16.5 m/s. Figs. 4 and 5 indicate that the number of
 266 particles measured by the LPM increased and the visibility decreased as the wind velocity increased.

267
 268 Table 1. Six events of moderately negative AEF/PG variation after a blizzard in 2015. They were

269 satisfied with the conditions that the number of particles measured by the LPM was less than 500
 270 and a negative AEF/PG was observed for more than 30 minutes. The start and end times of the
 271 negative AEF/PG after the blizzard are shown in the table. The minimum of the AEF/PG
 272 indicates the minimum value of the 5-minute running mean of the AEF/PG. The time constant τ
 273 is the period from the observed to the minimum value of the 5-minute running mean of the
 274 AEF/PG, $|E_{\min}|$, to the value of $|E_{\min}|/e$. The temperature refers to the hourly value observed
 275 during the negative AEF/PG.

	Date (2015)	Start time (UT)	End time (UT)	Duration [min.]	Min. of AEF/PG [V/m]	Time constant τ [minutes]	Lowest wind velocity [m/s]	Highest wind velocity [m/s]	Temperature [°C]
1	Feb. 8	3:57	4:48	52	-32.9	17	2.9	4.3	-3.8 (04UT)
2	Jul. 19	2:41	3:42	62	-39.4	36	5.9	7.1	-11.5 (03UT)
3	Jul. 19	4:39	5:24	46	-29.8	6	7.3	7.3	-12.0 (05UT)
4	Jul. 29	10:06	11:44	99	-101.2	58	3.8	8.2	-6.8 (14UT)
5	Aug. 10	16:06	17:21	76	-110.8	30	5.6	11.2	-15.7 (17UT)
6	Aug. 15	14:42	15:33	52	-63.1	14	5.3	8.9	-13.7 (15UT)

276



277

278 Fig. 6. Number of particles in different classes, AEF/PG, and wind velocity from 0000 UT to 2400
 279 on July 29, 2015. The color of the lines is the same as in Fig. 4. The blue and red bars denote the
 280 period of the blizzard and still images shown in Fig. 7, respectively.

281
282



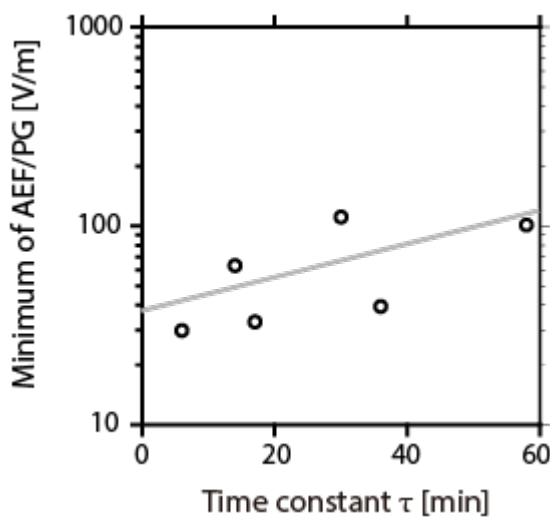
283
284 Fig. 7. Still images recorded every 5 minutes by the live camera from 0934 UT to 0959 UT on July
285 29, 2015.

286

287 Fig. 6 shows the time series of particle size distribution, AEF/PG values, and wind velocity from
288 0000 UT to 2400 UT on July 29, 2015. The blizzard ended at 0920 UT (Oshiki, 2016). The negative
289 AEF/PG started at 0952 UT, and the negative values remained from 1001 UT to 1238 UT.
290 Meanwhile, the NPP measured by the LPM at a height of 4.4 m was under 500. The recovery of
291 visibility was recognized from the still images shown in Fig. 7. The AEF/PG values reached a
292 minimum just after the blizzard ended and gradually recovered. The high-frequency fluctuation
293 was not found in the recovery period.

294 Thirty blizzards were identified at Syowa Station in 2015 (Yamamoto et al., 2015; Oshiki,
295 2016). Among them, six events of similar negative variations in AEF/PG were found, as shown in
296 Fig. 2. Table 1 lists the six events in 2015 that satisfied the conditions in which the negative
297 AEF/PG values remained for more than 30 minutes and the number of particles measured by the

298 LPM was less than 500. The date, start/end time, duration, minimum AEF/PG, time constant,
 299 lowest/highest wind velocity, and temperature for each event are also shown. The time constant τ
 300 for the recovery of the negative AEF/PG was estimated from the period of the observed minimum
 301 value of the 5-minute running mean of the AEF/PG, $|E_{\min}|$, to the value of $|E_{\min}|/e$, where e is the
 302 base of the natural logarithm. Although there was no significant correlation between the
 303 lowest/highest wind velocities or temperatures and the time constant τ , correlations between the
 304 minimum AEF/PG $|E_{\min}|$ and time constant τ were obtained. Fig. 8 illustrates the semi-logarithmic
 305 relationship of the time constant τ and the minimum of the 5-minute running mean of the AEF/PG
 306 $|E_{\min}|$. From these six events, the correlation coefficient between the time constant τ and the log
 307 $|E_{\min}|$ of the minimum AEF/PG was 0.65.



308
 309 Fig. 8. Relationship between the minimum value of the 5-minute running mean of the AEF/PG and
 310 the time constant τ in the six events satisfied the conditions that the number of particles measured
 311 by the LPM be less than 500 and a negative electric field was observed for more than 30 minutes,
 312 as listed in Table 1. The horizontal axis is the time constant τ , the period from the observed
 313 minimum value of the 5-minute running mean of the AEF/PG, $|E_{\min}|$, to the value of $|E_{\min}|/e$. The
 314 minimum value of the 5-minute running mean of the AEF/PG is logarithmically shown on the
 315 vertical axis. The gray line is a regression line. The correlation coefficient between the time
 316 constant τ and the log $|E_{\min}|$ is 0.65.

317

318 3. Calculations

319 Several previous papers have numerically investigated the electric field distribution formed by
 320 charged particles, such as snow and sand particles. Schmidt and Dent (1993) estimated the electric
 321 field intensity perpendicular to the surface when charged snow particles were arranged in a
 322 hexagonal configuration on the surface. They obtained an electric field of 1,000 V/m and 20 V/m
 323 at heights of 1–2 cm and 10 cm, not considering the charge of the snow particles suspended in the
 324 air. Gordon and Tylor (2009) proposed a model of the electric field formed by suspended snow

325 particles. They found that the electric field intensity was proportional to the particle number density
326 distribution in the model. However, the correlation coefficient r between the electric field intensity
327 and the snow-particle density in the field was relatively small, at $r^2 = 0.13$ to $r^2 = 0.66$. The
328 researchers concluded that the intensity of the electric field was likely influenced by various other
329 origins, such as snow conditions, the distribution of blowing snow density, and the history of
330 suspended particles. Zheng et al. (2004) constructed a theoretical model for calculating the electric
331 fields produced by charged sand particles, considering the saltation, suspension, and creep of the
332 particles. The result of the calculation, in which the charge-to-mass ratio of sand particles was -60
333 $\mu\text{C}/\text{kg}$, similar to the charge-to-mass ratio of snow particles, showed that an upward electric field
334 (i.e., a negative AEF/PG), exceeding $100 \text{ kV}/\text{m}$, was obtained just above the surface of the sand
335 layers. The electric field decreased quickly to zero, while the height increased. Then, the polarity
336 of the electric field changed (i.e., positive [downward]).

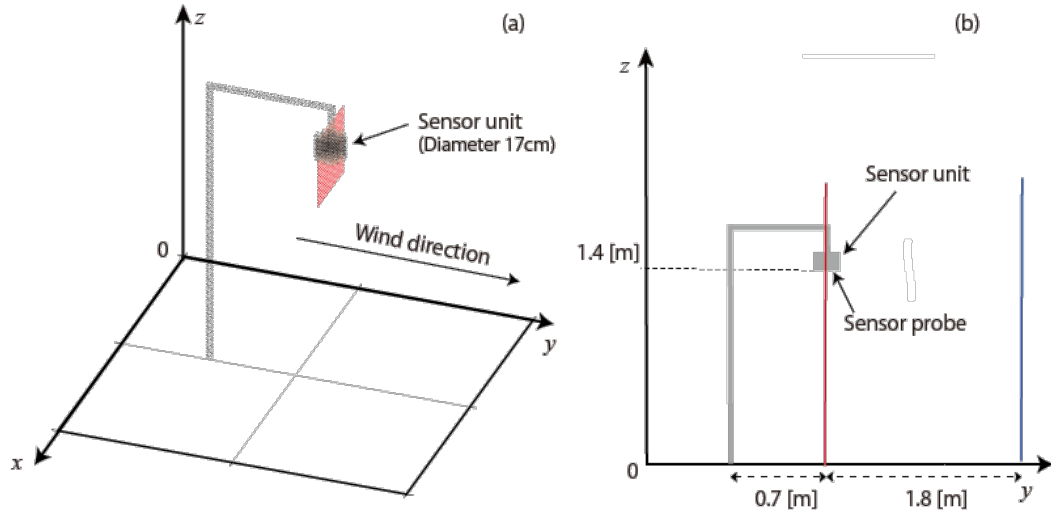
337 To verify the electric field distribution formed by the negatively charged snow particles
338 suspended in the snowstorm, we numerically solved the three-dimensional Poisson equation. This
339 is shown in equation (4):

$$340 \quad \frac{\partial^2 \varphi(x,y,z)}{\partial z^2} = -\frac{\rho(x,y,z)}{\epsilon_0} = -\frac{dE(x,y,z)}{dz}, \quad (4)$$

341 where $\varphi(x, y, z)$, $\rho(x, y, z)$, and $E(x, y, z)$ are the electric potential, charge density, and electric field,
342 respectively; x and y are the horizontal components; and z is the vertical height from the ground.

343 Although a downward (geocentric) direction is conventionally defined as positive in the
344 studies of atmospheric electricity, as introduced in Section 1, we define the upward direction as
345 positive in this numerical calculation. In this section, not AEF/PG but the electric field is used to
346 describe the calculated electric field in the Poisson equation because the horizontal components
347 are also required to calculate the electric field around the sensor.

348 The computational domain of 6 m in the horizontal direction (x and y components) and
349 2 m in the vertical direction (z -component) was set. Although the prevailing wind direction was set
350 in the y -axis (Fig. 9), the charge distribution $\rho(x, y, z)$ was regarded as uniform in the horizontal x
351 and y components because the constant wind velocity substantially carried the constantly charged
352 snow particles. In addition, the wind velocity concerned was much smaller than the electric field
353 propagation velocity (i.e., the velocity of light); the charge distribution was practically time-
354 independent (i.e., static). It must be noted that the electrical conductivity modification caused by
355 the snow particles was negligible; Shumilov et al. (2005) showed that no significant change in
356 atmospheric conductivity during the snowstorm was found at sites of high latitude in Russia. In the
357 calculations, the electric field mill and its metal mounting support (Fig. 1) are conductors and are
358 grounded, setting their potential to be zero and forming the boundary conditions shown in Fig. 9.
359 To reproduce the AEF/PG in fair weather (i.e., $100 \text{ V}/\text{m}$ in the geocentric direction), a positive
360 charge layer was installed at the top of the computational domain as a boundary condition.



361

362 Fig. 9. Conductor for the boundary condition (i.e., the sensor unit of the electric field mill and the
 363 pipe for mounting the sensor) shown in the Poisson calculation. The sensor was mounted at a height
 364 of 1.4 m. The cross-sections of the Poisson calculation results (shown in Figs. 11 and 13)
 365 correspond to the red plane in (a). The vertical component z of the Poisson calculation results
 366 (shown in Figs. 12 and 14) corresponds to the red and blue lines in (b). The computational domain
 367 is 6 m in the horizontal x - and y -directions and 2 m on the vertical z -axis.

368

369 The negative charge density originating from the snow particles was given as an initial condition,
 370 multiplying the number density distribution of the snow particles by the average amount of charge
 371 per snow particle. For simplicity, we assumed that the charge amount of each snow particle was
 372 constant. Omiya et al. (2011) measured the charge-to-mass ratios of snow particles at different
 373 temperatures and particle sizes in the wind tunnel experiment and estimated that the electric charge
 374 per snow particle was -2×10^{-14} C under the conditions of air temperature at -10 C and a particle
 375 size of 0.3 mm. The median charge per snow particle at Byrd Station was -5×10^{-14} C when the
 376 wind velocity at the height of 50 cm was between 4.5 and 6.5 m/s (Wishart, 1968).

377

378 Fifty-seven percent of the wind direction was north-northeast, northeast, and east-
 379 northeast at Syowa Station (Sato and Hirasawa, 2007). Northeast wind prevailed during blizzards.
 380 When maximum wind speed was observed, the wind directions were north-northeast, northeast,
 381 and east-northeast in 29 out of the 30 blizzards identified in 2015 at Syowa Station (Yamamoto et
 382 al., 2015; Oshiki, 2016). The ocean extends to the northeast of Syowa Station. The sea surface was
 383 frozen during the period of analysis in this paper (Ushio, 2015; Miura, 2016). During the blizzard,
 many snow particles were negatively charged because they migrated into Syowa Station with

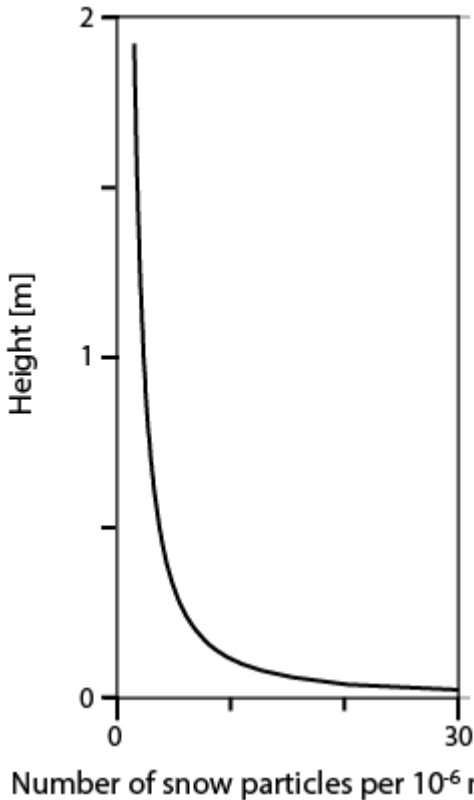
384 repeated saltations at the snow surface on the sea ice. The charge amount of the snow particles
 385 depends on the transported length with snow surface collisions (Omiya and Sato, 2011). This
 386 implies that the charge accumulated with multi-collisions. Therefore, we considered the possibility
 387 that the charge amount in the calculation would be larger and smaller than that in previous studies
 388 (Wishart, 1968; Omiya and Sato, 2011). The charge amounts were given by -1×10^{-13} , -1×10^{-14} ,
 389 and -1×10^{-15} C per snow particle.

390 We used the density distribution of snow particles observed at Halley Station, Antarctica,
 391 obtained by Mann et al. (2000). They measured the snow-particle number flux and presented the
 392 10-minute mean profile of snow particle number density into eight wind speed bins ranging
 393 between 10 and 17 m/s (1.0 m/s bin width). These profiles showed that the number density of snow
 394 particles decreased with height following a power law. We formulated the number of snow particles
 395 per unit volume, $n_w(z)$, as a function of height, z , for each wind velocity bin w , as depicted in Mann
 396 et al. (2000), with the constant values a_w and b_w shown as follows:

$$397 \quad n_w(z) = 10^{k_w(z)}, \text{ where } k_w(z) = a_w z + b_w. \quad (5)$$

398 For $w = 15\text{--}16$ m/s, we derived the coefficients of $a_w = -0.67$ and $b_w = 6.37$. Fig. 10 shows the
 399 height distribution of the number of snow particles per 10^{-6} m^3 (1 cm^3).

400



401

402 Fig. 10. Height distribution of the number density of snow particles depicted in Mann et al. (2000)
 403 for the Poisson calculation. The horizontal and vertical axes denote the number of snow particles
 404 per 10^{-6} m^3 and the height (i.e., z), respectively.

405

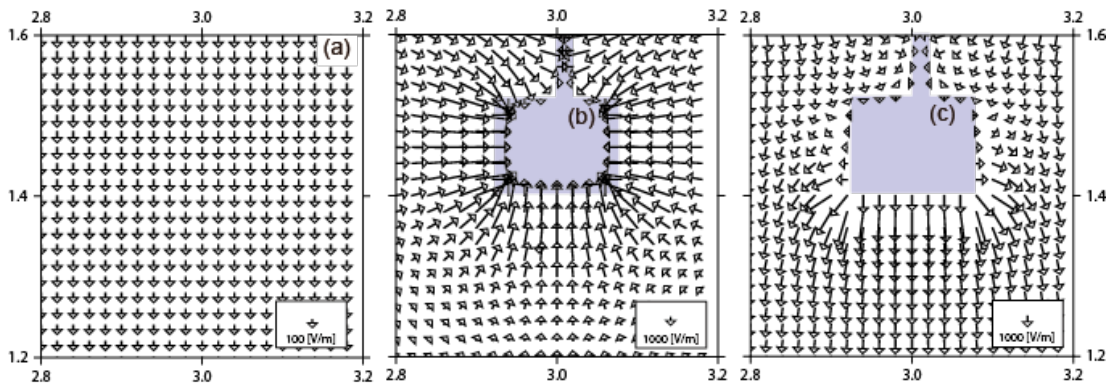
406 The sensor of the electric field mill was installed at 1.4 m in height and mounted downward using
407 a metal pipe (Fig. 1). The measured value of the grounding resistance of the sensor was 100 Ω .
408 Assuming that the constant permittivity and conductivity of the snow surface are ε and κ , the
409 relaxation time T_{relax} is represented by the following equation (Harrison et al., 2016):

410
$$T_{relax} = \varepsilon/\kappa. \quad (6).$$

411 Gow (1968) sampled snow and ice on the surfaces and in the boreholes at several sites in Antarctica
412 and Greenland and measured their electric conductivity. The conductivity of the snow and ice was
413 1 to 2×10^{-4} S/m at inland sites. The conductivity at Little America V ($78^{\circ}11'S, 162^{\circ}12'W$), located
414 on the Ross Ice Shelf near the sea, was about 6×10^{-4} S/m. The relative permittivity measured at a
415 depth of 1 m in Antarctica was between 1.4 and 2.0 (Sugiyama et al., 2010). Since the permittivity
416 of the air was 8.9×10^{-12} F/m when the conductivity was assumed to be 10^{-4} , the relaxation time
417 was about 10^{-7} seconds, which was negligible. The sensor unit of the electric field mill and the
418 metal pipe mounting the sensor unit (Fig. 9) were grounded. The three-dimensional Poisson
419 calculations were carried out with the above charge and conductor distribution as initial and
420 boundary conditions.

421 Fig. 11 shows the electric field distribution on the plane (red plane in Fig. 9a) across the sensor
422 unit of the electric field mill. The electric field in fair weather without and with the sensor unit is
423 shown in Fig. 11a and b, respectively. Fig. 11c shows the electric field with the sensor unit in the
424 distribution of snow particles (i.e., during the blizzard), based on the observation of Mann et al.
425 (2000). The electric charge was -1×10^{-14} C per snow particle.

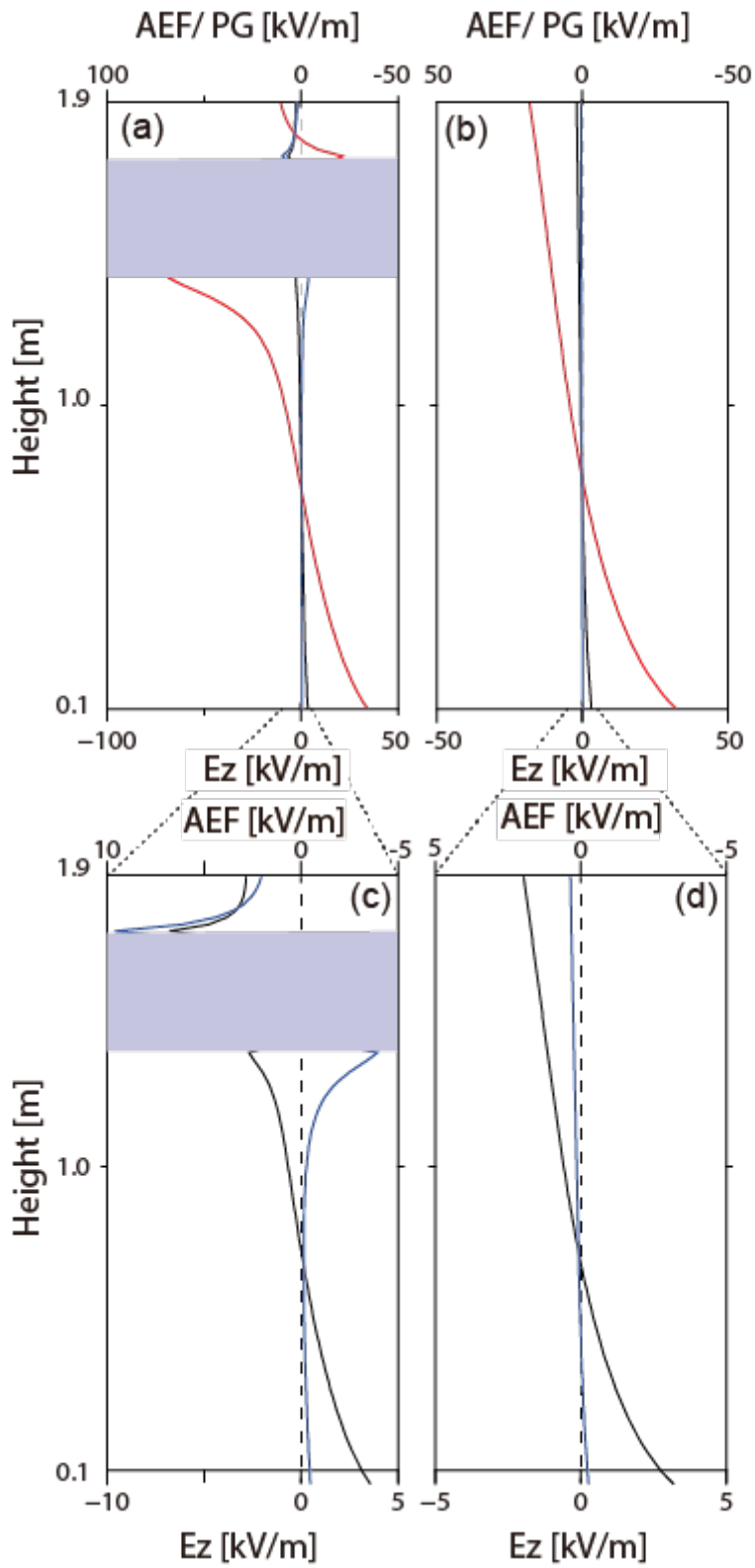
426



427

428 Fig. 11. Electric field in the three-dimensional Poisson calculation. A cross-section (red plane in
429 Fig. 9a) across the sensor unit is shown. The arrows indicate the direction and magnitude of the
430 electric field. The area of the conductor corresponding to the sensor unit and metal pipe is shaded.
431 The calculation results are as follows: (a) in fair-weather without the sensor unit, (b) in fair-weather
432 with the sensor unit, and (c) during the blizzard with the electric charge amount of -1×10^{-14} C per
433 snow particle, with the sensor unit.

434



435
 436 Fig. 12. Vertical distribution of the z-component of the electric field in the three-dimensional
 437 Poisson calculation. The number density of snow particles during the blizzard as an initial
 438 condition was based on Mann et al. (2000). The red, black, and blue lines indicate the calculation
 439 results for the charge amounts of -1×10^{-13} , -1×10^{-14} , and -1×10^{-15} C per snow particle,

440 respectively. (a), (b) The z -component of the electric field along a vertical line (red line in Fig.
441 9b) through the sensor unit. There is a conductor of the sensor unit from 1.4 m to 1.7 m in height.
442 (c), (d) The z -component of the electric field along a vertical line (blue line in Fig. 9b), not
443 passing through the sensor unit. The wide and narrow ranges of the AEF/PG are shown in (a), (c),
444 and (b), (d), respectively.

445

446 When the direction of the electric field is from outside to inside the sensor electrode of
447 the electric field mill, it is positive. In other words, the arrows heading to the field mill at the
448 undersurface of the sensor indicate a fair-weather electric field. Fig. 11b shows the calculated
449 electric field reproducing the positive electric field in fair weather. Conversely, the electric field
450 heading away from the sensor electrode was measured as a negative electric field. The result of the
451 calculation shown in Fig. 11c during the blizzard did not provide the electric field heading away to
452 the sensor unit. From this result, the negative electric field was expected to be measured by the
453 calculation but not observed in the field. Therefore, the intense positive electric field observed
454 during the blizzard, shown in Figs. 4 and 6, was not reproduced.

455 Fig. 12 shows the distribution of the electric field on the z -axis during the blizzard. The
456 z component of the calculated electric field on the vertical line passing through the sensor unit (red
457 line in Fig. 9b) and on the line not passing through the sensor unit (blue line in Fig. 9b) are shown
458 in Fig. 12a and 12b, respectively. The calculation results with electric charge amounts of -1×10^{-13} ,
459 -1×10^{-14} , and -1×10^{-15} C per snow particle are shown as red, black, and blue lines, respectively.
460 The electric field of the z -component was negative, and this corresponds to arrows heading away
461 at the undersurface of the sensor just below the electric probe of the sensor unit in Fig. 11. In this
462 case, the output value of the electric field mill was negative. The magnitude of the electric field
463 varied widely depending on the charge amount of the snow particles.

464 The electric field showed a downward direction just below the electric probe of the
465 sensor unit, corresponding to the electric field from the inside to the outside of the sensor unit, as
466 shown in Fig. 11. In this case, the output value measured by the electric field mill was negative.
467 The magnitude of the electric field varied widely depending on the charge amount of the snow
468 particles.

469

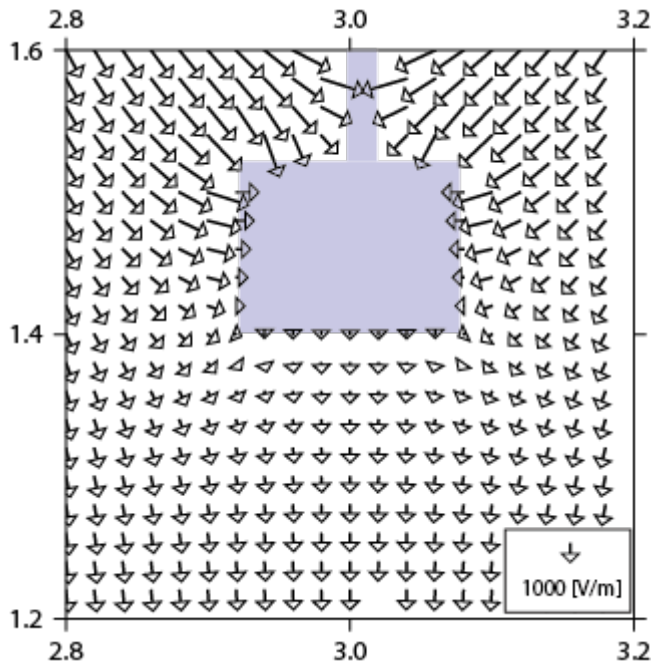
470 **4. Discussion**

471 The observed AEF/PG values and calculated electric field values during blizzards were
472 different. The installation method for the electric field mill is described in Section 6.1.2 of
473 MacGorman and Rust (1998). They mentioned that the electric probe of the sensor unit facing
474 downward into the ground (inverted sensor) effectively avoided the electrical noise caused by the
475 charged particles attached to the sensor when charged particle precipitation, such as rain and snow,
476 was falling. Ogawa (1973) estimated that the electric field caused by rain precipitation was 1 kV/m,

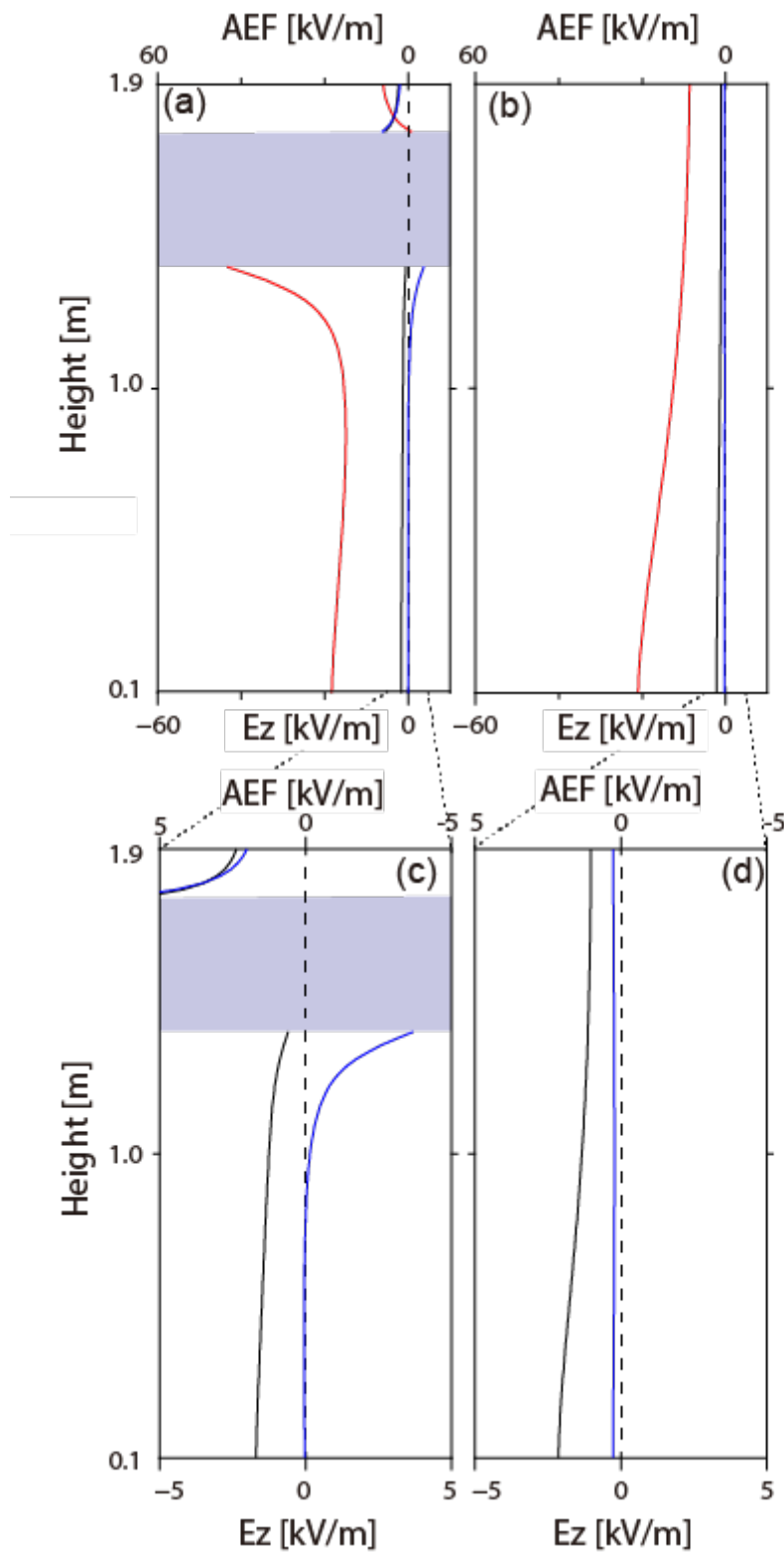
477 based on the measurement of the electric current generated by raindrops reported by Ogawa (1960).
478 From the estimation, the polarity of the electric field was opposite to that of the charge of the
479 raindrops. Moreover, the inverted sensor in the condition of the blizzard was ineffective at avoiding
480 the charged snow particles attaching to the sensor because the suspended and saltating snow
481 particles were reachable, even to the inverted sensor. Thus, we concluded that the positive intense
482 AEF/PG values observed during the blizzard were apparent electric field measurements because
483 of collisions of charged snow particles with the sensor electrodes.

484 After a blizzard, the suspended and saltating snow particles fell onto the snow surface
485 with a negative charge. Although the relaxation time of the charge on the solid snow surface was
486 negligible, as shown in equation (6), the charged snow particles softly attaching to the surface took
487 a certain time to discharge. Sims et al. (2003) calculated the discharge decay-time constant (i.e.,
488 the time to reach the charge of $1/e$) for various powders on the surface. The discharge decay times
489 of the Mars dust simulants and acrylic polymer powders were about 5 minutes and 150 minutes,
490 respectively. We carried out the Poisson calculation under the initial condition that a thin layer of
491 negatively charged snow particles was covered on the snow surface (Figs. 13 and 14). The results
492 of the Poisson calculations shown in Fig. 13 indicated that when the negative charge density for
493 the thin layer on the surface was $-1 \times 10^{-8} \text{ C/m}^2$, an electric field heading away from the field mill
494 sensor was reproduced. Fig. 14 shows that when the negative charge density was $-1 \times 10^{-7} \text{ C/m}^2$
495 or $-1 \times 10^{-8} \text{ C/m}^2$, the calculated electric field was opposite to that of $-1 \times 10^{-9} \text{ C/m}^2$. Assuming
496 that the distribution of the number density of snow particles followed that of Mann et al. (2000)
497 and that the electric charge per snow particle was $-1 \times 10^{-14} \text{ C}$, the charge density layer on the
498 surface became $-5.5 \times 10^{-8} \text{ C/m}^2$ when the suspended and saltating snow with the negative charge
499 from the ground to 1.0 m fell into the surface.

500



501
 502 Fig. 13. Electric field with the negatively charged snow-particle layer on the surface of -1×10^{-8}
 503 C/m^2 on the cross-section (red plane in Fig. 9a) across the sensor unit is shown. The arrows
 504 indicate the direction and magnitude of the electric field. The area of the conductor
 505 corresponding to the sensor unit and metal pipe is shaded.
 506



507

508 Fig. 14. Vertical distribution of the electric field z-component with the initial condition of which
 509 the negatively charged snow particle layer on the surface is shown. The red, black, and blue lines
 510 indicate the calculation results, in which the charge densities are -1×10^{-7} , and -1×10^{-8} C/m²,
 511 -1×10^{-9} , respectively. (a), (b) The z-component of the electric field along a vertical line (red

512 line in Fig. 9b) through the sensor unit. There is a conductor of the sensor unit from 1.4 m to 1.7
513 m in height. (c), (d) The z-component of the electric field along a vertical line (blue line in Fig.
514 9b), not passing through the sensor unit. The wide and narrow ranges of the AEF/PG are shown
515 in (a), (c), and (b), (d), respectively.

516

517 The live camera was located more than 100 m away from the sensor unit of the electric field mill.
518 The height of the camera (30 m) was higher than that of the electric field mill sensor (1.4 m).
519 Therefore, it was difficult for the still images recorded by the camera to verify the presence of
520 powdered snow on the ground because of insufficient image resolution. The LPM sensor for
521 measuring the NPP, shown in Figs. 4 and 6, was mounted at a height of 4.4 m, and the snow
522 particle layer was not measured. However, the origin of the negative electric field just after the
523 blizzard was explained, assuming that the presence of the snow-particle layer originated from the
524 falling of suspended and saltating snow particles to the ground.

525 We found a correlation between the duration of the negative AEF/PG and the magnitude
526 of the electric field: The larger the magnitude of the negative electric field value was, the longer
527 the duration of the negative AEF/PG value became. This correlation was understandable when we
528 speculated about the relationship between the time required for the discharge of the snow particles
529 softly attaching to the snow surface and the amount of electric charge of the snow particles.
530 However, monitoring the distribution of snow particles and the electric charge of the particles just
531 above the ground surface may enable us to verify this speculation, as it remains a problem for
532 future consideration.

533 Although the electric field mill is generally used for the observation of AEF/PG, the
534 measurements do not reflect the signal originating from the charged particle distribution,
535 particularly under severe conditions, such as in desert and polar regions. Nicoll et al. (2020)
536 observed a positive AEF/PG exceeding 7 kV/m, generated by charged desert dust at Al Ain in the
537 United Arab Emirates. Renno et al. (2008) developed an electric field mill for Mars. They
538 mentioned that a typical dust storm on Mars, such as with a charge density of 10^{-8} C/m^3 and a wind
539 velocity of 20 m/s, generates an electric field of about 11 kV/m. Therefore, to monitor the AEF/PG
540 in a dusty environment, signals caused by the collisions of charged particles must be discriminated
541 from the signal of ambient AEF/PG. Furthermore, the measurements of the electric field mill are
542 applicable to automatic storm monitoring because the magnitude of the measured noise is possibly
543 correlated to that of the storm. For instance, the start and end times of blizzards, such as the events
544 at Syowa Station, have generally been identified from ocular observation. However, the electrical
545 observation using the field mill offers unmanned monitoring because the intense positive electric
546 field may be related to visibility. In further application, observations with the field mill were also
547 useful for snow drifting studies in areas with high mountains, such as the Alps and Mt. Fuji, to
548 mitigate snow avalanches (Gauer, 2001) and turbulent electrification monitoring for industrial dust

549 to avoid explosions.

550

551 **5. Conclusion**

552 We investigated the origin of the intense positive AEF/PG during blizzards/snowstorms and the
553 moderate negative AEF/PG just after a blizzard at Syowa Station, Antarctica. A Poisson calculation
554 with the negatively charged snow particles surrounding the sensor unit did not reproduce the
555 observed intense positive AEF/PG during the blizzard. This implies that the intense positive PG
556 during the blizzard should be the apparent electric field variation originating from the suspended
557 and saltating snow particles attached to the sensor. The moderate negative AEF/PG just after the
558 blizzard was reported for the first time. When a moderate negative electric field was observed, the
559 number of snow particles dropped at a point higher than the sensor unit of the electric field mill.
560 We modeled that the charge of the snow particles that had fallen and softly attached to the ground
561 on the ground surface remained during the negative AEF/PG. The Poisson calculation in the model
562 reproduced the negative electric field. Thus, we showed that the origins of the intense positive and
563 moderate negative electric fields during and after blizzards are the charged snow particles colliding
564 with the electric probe on the sensor unit and the negative snow layers softly attached to the ground.

565

566 **Acknowledgments**

567 The authors thank Y. Kimura, Y. Suzuki, and T. Ishikawa (Tokyo Gakugei University) for their help
568 and discussion. The Japan Meteorological Agency (JMA) provides 1-minute wind velocity data.
569 The AEF data are provided by the University of Shizuoka and the National Institute of Polar
570 Research (NIPR), Japan. The data on the NPPs and time-lapse images are provided by the National
571 Institute of Polar Research (NIPR). Fig. 1 was created using the map “Syowa Station” at a scale of
572 1:2,500 by the Geographical Survey Institute of Japan. This study was part of the Science Program
573 (AP41 and AP905) of the Japanese Antarctic Research Expedition (JARE; YM, MK, AK, and SM).
574 It was supported by NIPR under MEXT and NIPR through General Collaboration Project No. 23-
575 12 (YM, MK, and AK), 26-13 (YM, MK, AK, and SM), and 29-15 (YM, MK, AK, and SM). The
576 authors are grateful to the JARE members for their efforts to maintain the AEF and other
577 observation equipment at Syowa Station. This research was also supported in part by the Joint
578 Support-Center for Data Science Research ROIS-DS-JOINT 2018 and 2020 (YM, MK, AK, and
579 SM), research project no. 2019-01 (YM, MK, AK, and SM), Institute of Oceanic Research and
580 Development, Tokai University (MK), and JSPS KAKENHI Grant Number 20H02419 (MK).

581

582

583 **References**

584 Aplin, K.L., 2018. Atmospheric electricity at Durham: the scientific contributions and legacy of
585 JA (“Skip”) Chalmers (1904–1967). *Hist. Geo Space. Sci.* 9(1), 25–35.

586 Anderson, R.S., 1987. Eolian sediment transport as a stochastic process: the effects of a
587 fluctuating wind on particle trajectories. *J. Geol.* 95, 497–512.

588 Asuma, Y., Kikuchi, K., Taniguchi, T., Fujii, S., 1988. Vertical structures of the atmospheric
589 electrical potential gradient and the behavior of the precipitation charges during snowfalls near
590 the ground surface. *J. Meteorol. Soc. Jpn. Ser. II.* 66, 473–488.

591 Burrows, D.A., Hobbs, P.V., 1970. Electrical charges on snow particles. *J. Geophys. Res.* 75,
592 4499–4505.

593 Gauer, P., 2001. Numerical modeling of blowing and drifting snow in Alpine terrain. *J. Glaciol.*
594 47, 97–110.

595 Gordon, M., Taylor, P.A., 2009. Measurements of blowing snow, part I: particle shape, size
596 distribution, velocity, and number flux at Churchill, Manitoba, Canada. *Cold Reg. Sci.*
597 *Technol.* 55, 63–74.

598 Gow, A.J., 1968. Electrolytic conductivity of snow and glacier ice from Antarctica and
599 Greenland. *J. Geophys. Res.* 73, 3643–3649.

600 Harrison, R.G., 2004. The global atmospheric electrical circuit and climate. *Surv. Geophys.* 25,
601 441–484.

602 Harrison, R.G., 2013. The carnegie curve. *Surv. Geophys.* 34, 209–232.

603 Harrison, R.G., Barth, E., Esposito, F., Merrison, J., Montmessin, F., Borlina, C., Berthelie, J.J.,
604 Deprez, G., Farrell, W.M., Houghton, I.M.P., Renno, N.O., Nicoll, K.A., Tripathi, S.N.,
605 Zimmerman, M., 2016. Applications of electrified dust and dust devil electrostatics to
606 Martian atmospheric electricity. *Space Sci. Rev.* 203, 299–345.

607 Hirasawa, N., Konishi, H., Nishimura, K., Genthon C., 2018. Project group of Japan
608 Meteorological Agency, SPICE site report: Rikubetsu, Japan. WMO Solid Precipitation
609 Intercomparison Experiment SPICE 2012–2015. Instruments and Observing Methods, Report
610 No. 131.

611 Kikuchi, K., 1970. Observations of the AEF at Syowa Station, Antarctica. *J. Meteorol. Soc. Jpn.*
612 *Ser. II.* 48, 452–460.

613 Latham, J., Montagne, J., 1970. The possible importance of electrical forces in the development
614 of snow cornices. *J. Glaciol.* 9, 375–384.

615 Liu, C., Williams, E.R., Zipser, E.J., Burns, G., 2010. Diurnal variations of global thunderstorms
616 and electrified shower clouds and their contribution to the global electrical circuit. *J. Atmos.*
617 *Sci.*, 67, 309–323.

618 MacGorman, D.R., Rust, W.D., 1998. *The Electrical Nature of Storms.* Oxford University Press,
619 London.

620 Maeno, N., Naruse, R., Nishimura, K., Takei, I., Ebinuma, T., Kobayashi, S., Nishimura H.,
621 Kaneda Y., Ishida, T., 1985. Wind-tunnel experiments on blowing snow. *Ann. Glaciol.* 6, 63–
622 67.

- 623 Mann, G.W., Anderson, P.S., Mobbs, S.D., 2000. Profile measurements of blowing snow at
624 Halley, Antarctica. *J. Geophys. Res. Atmos.* 105, 24491–24508.
- 625 Markson, R., 2007. The global circuit intensity: its measurement and variation over the last 50
626 years. *Bull. Amer. Meteor.* 88, 223–241.
- 627 Minamoto, Y., Kadokura, A., 2011. Extracting fair-weather data from atmospheric electric-field
628 observations at Syowa Station, Antarctica. *Polar Sci.* 5, 313–318.
- 629 Miura, H., 2016. Conditions of weather and sea ice, JARE-56 Report. The 56th Japanese
630 Antarctic Research Expedition Eds. 136–137. (in Japanese).
- 631 Nemoto, M., Nishimura, K., 2004. Numerical simulation of snow saltation and suspension in a
632 turbulent boundary layer. *J. Geophys. Res. Atmos.* 109, D18206.
- 633 Nicoll, K.A., Harrison, R.G., Barta, V., Bor, J., Brugge, R., Chillingarian, A., Chum, J.,
634 Georgoulas, A.K., Guha, A., Kourtidis, K., Kubicki, M., Mareev, E., Matthews, J., Mkrtchyan,
635 H., Odzimek, A., Raulin, J.-P., Robert, D., Silva, H.G., Tacza, J., Yair, Y., Yaniv, R., 2019. A
636 global atmospheric electricity monitoring network for climate and geophysical research. *J.*
637 *Atmos. Sol.-Terr. Phys.* 184, 18-29.
- 638 Nicoll, K., Harrison, G., Marlton, G., Airey, M., 2020. Consistent dust electrification from
639 Arabian Gulf sea breezes. *Environ. Res. Lett.*, 15, 084050.
- 640 Ogawa, T., 1960. Electricity in rain. *J. Geomag. Geoelec.* 121, 21–31.
- 641 Ogawa, T., 1973. Analyses of measurement techniques of electric field and currents in the
642 atmosphere. *Contrib. Geophys. Inst., Kyoto Univ.* 13, 111–137.
- 643 Omiya, S., Sato A., 2011. Wind tunnel experiment of an electrostatic charge of blowing-snow
644 particles focusing on collision frequency to the snow surface. *Seppyo.* 73, 205–212. (in
645 Japanese with English abstract).
- 646 Omiya, S., Sato, A., Kosugi, K., Mochizuki, S., 2011. Estimation of the electrostatic charge of
647 individual blowing-snow particles by wind tunnel experiment. *Ann. Glaciol.* 52, 148–152.
- 648 Oshiki, N., 2016. Weather analyses, JARE-56 Report. The 56th Japanese Antarctic Research
649 Expedition Eds. 252–255. (in Japanese).
- 650 Renno, N.O., Kok, J.F., Kirkham, H., Rogacki, S., 2008. A miniature sensor for electrical field
651 measurements in dusty planetary atmospheres. *J. Phys. Conf. Ser.* 142, 012075.
- 652 Sato, K., Hirasawa, N., 2007. Statistics of Antarctic surface meteorology based on hourly data in
653 1957–2007 at Syowa Station. *Polar Sci.* 1, 1–15.
- 654 Schmidt, D.S., Dent, J.D., 1993. A theoretical prediction of the effects of electrostatic forces on
655 saltating snow particles. *Ann. Glaciol.* 18, 234–238.
- 656 Schmidt, D.S., Schmidt, R.A., Dent, J.D., 1999. Electrostatic force in blowing snow. *Bound-lay*
657 *Meteorol.* 93, 29–45.
- 658 Shumilov, O.I., Kasatkina, E.A., Kulichkov, S.N., Kallistratova, M.A., Vasil'ev, A.N., 2005.
659 Meteorological effects in the atmospheric electric field in the high latitudes. *Izvestiya Atmos.*

660 Oceanic Phys. 41, 555–562.

661 Sims, R.A., Biris, A.S., Wilson, J.D., Yurteri, C.U., Mazumder, M.K., Calle, C.I., Buhler, C.R.,
662 2003. Development of a transparent self-cleaning dust shield for solar panels. Proc. ESA-IEEE
663 Joint Meeting on Electrostatics. 814–821.

664 Sugiyama, S., Enomoto, H., Fujita, S., Fukui, K., Nakazawa, F., Holmlund, P., 2010. Dielectric
665 permittivity of snow measured along the route traversed in the Japanese–Swedish Antarctic
666 Expedition 2007/08. *Ann. Glaciol.* 51, 9–15.

667 Suzuki, T., Matsudo, Y., Asano, T., Hayakawa, M., Michimoto, K., 2011. Meteorological and
668 electrical aspects of several winter thunderstorms with sprites in the Hokuriku area of Japan. *J.*
669 *Geophys. Res. Atmos.* 116, D06205.

670 Tsurudome, C., Flaquiere, A., Mochizuki, K., Teuff, Y., Sakai, R., Tuffenis, J., Suzuki, Y., Cohen,
671 D., Fujiwara, H., Inazaki, K., Yahi, S., Nakamura, M., Kamogawa, M. (2013). Measurement of
672 the atmospheric electric field inside the nonthunderstorm clouds on 2012 BEXUS campaign. *J.*
673 *Atmos. Electr.* 33, 77–80.

674 Ushio S., 2015. Conditions of weather and sea ice, JARE-55 Report. The 55th Japanese Antarctic
675 Research Expedition Eds. 147–148. (in Japanese).

676 Williams, E., Mareev, E., 2014. Recent progress on the global electrical circuit. *Atmos. Res.* 135,
677 208–227.

678 Wishart, E.R., 1968. Electrification of Antarctic drifting snow. Proc. Int. Symp. Antarctic
679 Glaciological Exploration, Hanover 86, 316–324.

680 World Meteorological Organization, 1966. International Meteorological Vocabulary. Secretariat
681 of the World Meteorological Organization.

682 Yamamoto, H., Imaizumi, K., Asahara, N., Ohtake, J., Saeki, Y., 2015. Weather, JARE-55 Report.
683 The 55th Japanese Antarctic Research Expedition Eds. 225–242. (in Japanese).

684 Zheng, X., He, L., Zhou, Y., 2004. Theoretical model of the electric field produced by charged
685 particles in windblown sand flux. *J. Geophys. Res. Atmos.* 109, D15208.